

GTA: Global Temporal Attention for Video Action Understanding

Bo He^{1*}, Xitong Yang^{1*}, Zuxuan Wu^{1,2}, Hao Chen¹, Ser-Nam Lim², Abhinav Shrivastava¹

¹University of Maryland, College Park ²Facebook AI

{bohe, xyang35, zxwu, chen, abhinav}@cs.umd.edu, sernamlim@fb.com

Abstract

Self-attention learns pairwise interactions via dot products to model long-range dependencies, yielding great improvements for video action recognition. In this paper, we seek a deeper understanding of self-attention for temporal modeling in videos. In particular, we demonstrate that the entangled modeling of spatial-temporal information by flattening all pixels is sub-optimal, failing to capture temporal relationships among frames explicitly. We introduce Global Temporal Attention (GTA), which performs global temporal attention on top of spatial attention in a decoupled manner. Unlike conventional self-attention that computes an instance-specific attention matrix, GTA randomly initializes a global attention matrix that is intended to learn stable temporal structures to generalize across different samples. GTA is further augmented with a cross-channel multi-head fashion to exploit feature interactions for better temporal modeling. We apply GTA not only on pixels but also on semantically similar regions identified automatically by a learned transformation matrix. Extensive experiments on 2D and 3D networks demonstrate that our approach consistently enhances the temporal modeling and provides state-of-the-art performance on three video action recognition datasets.

1. Introduction

Attention mechanisms have demonstrated impressive achievements in a wide range of tasks such as language modeling [1, 2], speech recognition [3] and image classification [4, 5]. One of the most effective attention methods is self-attention, which uses query-key-value dot product to capture long-range dependencies among tokens [2], and image pixels [6]. This makes self-attention particularly appealing for action recognition, which at its core aims to model temporal dependencies among frames. However, existing methods [6, 7] use self-attention by flattening pixels in space and time into a huge vector to build a dense graph.

*indicates equal contribution.

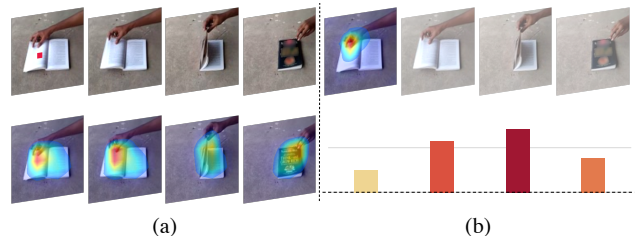


Figure 1: (a) **Top**: frame sequence (action: closing something). The red mark indicates the query position for spatio-temporal self-attention. **Bottom**: attention maps generated by the non-local module. The attention map is biased towards the appearance similarity and the temporal context is dominated by the spatial one. (b) Attention maps generated by the proposed decoupled non-local module. **Top**: spatial attention map. **Bottom**: temporal attention weights on different time steps. The temporal attention focuses more on keyframes that are critical for recognizing the action.

This incurs both quadratic memory consumption and time complexity with respect to the length of the vector.

The key components to self-attention are learning self-alignment via dot product operations, computing pairwise similarities between a pixel (*i.e.*, query) and other pixels (*i.e.*, key) to modulate the transformed inputs (*i.e.*, value). For action recognition, this requires that all pixels in a video, regardless of their spatial and temporal locations, share the same set of parameters to derive the query, key, and value. In this paper, we seek a better understanding of self-attention for temporal modeling in videos. In particular, we wish to answer the following questions: (1) Is treating all pixels in space and time as a flattened vector to perform dot-product sufficient for temporal modeling? (2) Is dot product based self-attention really necessary for capturing temporal relationships across different frames?

In contrast to the conventional use of self-attention for video recognition, we posit that temporal attention should be disentangled from spatial attention, since they focus on different aspects. As shown in Figure 1(b), the spatial attention (top row) tends to capture appearance similarities (*i.e.*, the book), while the temporal attention (bottom row)

is more focused on frames that are important for recognizing the action (*i.e.*, closing the book). When these two types of attention are modeled together (Figure 1(a)), the attention map is biased towards the appearance similarity, dominating any temporal context.

In addition, we argue that dot product based self-attention is *not even suitable* for temporal modeling. Standard self-attention produces instance-specific attention weights, conditioned on pairwise interactions. In the spatial domain, it is able to attend to salient regions for improved performance. When used for temporal modeling, it ignores the ordering of frames as self-attention is known to be permutation invariant [8]. For instance, if we shuffle two pixels temporally, their relationship will be the same as before, producing the same output. This is not sufficient for differentiating actions like “open a book” and “close a book”. We hypothesize that temporal modeling requires learning a global temporal structure that generalizes across different samples rather than relying on pairwise interactions across time steps.

In light of this, we introduce Global Temporal Attention (GTA), for video action recognition. In particular, we first decouple the traditional spatial-temporal self-attention into two successive steps—a standard self-attention in the spatial domain within each frame followed by the proposed GTA module to capture temporal relationships across different frames. Unlike computing pairwise frame interactions with dot product, we randomly initialize a global attention matrix to be instance-independent. The intuition of the global attention matrix is to not rely on pairwise frame relations without specific ordering information or individual sample information, but to learn a global task-specific weight matrix considering temporal structures among samples. To exploit information across different channels, we split feature maps into multiple groups along the channel-dimension, and for each group we apply GTA in a multi-head fashion such that each head focuses on different aspects of the inputs. Then, outputs from different channel groups are further aggregated to produce a unified representation. In addition, we not only apply GTA to each pixel location along the temporal dimension but also “superpixels”—pixels in a region share similar semantic meanings. This is achieved by learning a transformation matrix which converts pixels in a frame into multiple regions automatically.

We conduct extensive experiments on Something-Something dataset [9] (both v1 and v2) and Kinetics-400 dataset [10]. Our experimental results demonstrate that our proposed GTA outperforms the traditional spatial-temporal self-attention module by clear margins, and achieves state-of-the-art results on these three datasets.

We summarize our main contributions as follows. First, we demonstrate that conventional self-attention is not suit-

able for temporal modeling in action recognition. Second, we introduce GTA, which learns a global attention matrix for all samples instead of computing pairwise frame relationships by dot product. Third, we use GTA in a multi-head fashion across different channel groups for improved temporal modeling. Finally, we apply GTA on the pixel-level and region-level to learn complementary temporal relationships, and achieve state-of-the-art performance on three action benchmarks.

2. Related Work

Temporal Modeling in Action Recognition. A large family of research in action recognition focuses on effective modeling of the temporal information in videos. Early work simply aggregates the frame/clip-level features across time via average pooling [11, 12] or feature encoding like ActionVLAD [13], without considering the temporal ordering of video frames. Later on, 3D convolution networks (CNNs) [14, 15], recurrent neural networks (RNNs) [16, 17] are used to model the spatial and temporal context in videos. Recently, some temporal modules are proposed to capture temporal relations for action recognition, such as TRN [18] based on relation networks, Non-local Network [6] based on self-attention, Timeception [19] based on multi-scale temporal convolutions, and SlowFast [7] based on slow and fast branches capturing spatial and motion information, respectively. Instead of using temporal convolutions, TSM [20] adopts a channel shifting operation along the time dimension to enable temporal modeling on 2D CNN networks. Similar to the non-local network, our work presents a way to model temporal relationships using attention mechanisms, but GTA learns a global temporal attention that generalizes well across different samples as opposed to using pairwise interactions with dot product.

Non-Local and Self-Attention. Modeling non-local relations in feature representations has a long history [21–26] and has proven to be effective in various tasks, such as machine translation [2], generative modeling [27], image recognition [5, 6, 28], object detection [6, 28, 29], semantic segmentation [6, 28, 30] and visual question answering [31]. The most related work is Non-local Network [6] which models the pixel-level pairwise similarities to encode long-range dependencies. SENet [4] uses a Squeeze-and-Excitation block to model inter-dependencies along the channel dimension. DANet [32] computes pixel-wise and channel-wise attention to strengthen feature maps in the semantic segmentation task. GCNet [28] simplifies the NL block and combines it with SENet. CCNet [33] captures the contextual information of the pixels on its crisscross path instead of the global region in a more efficient way. In this paper, we show improvements over the non-local self-attention and bring new perspectives for a better under-

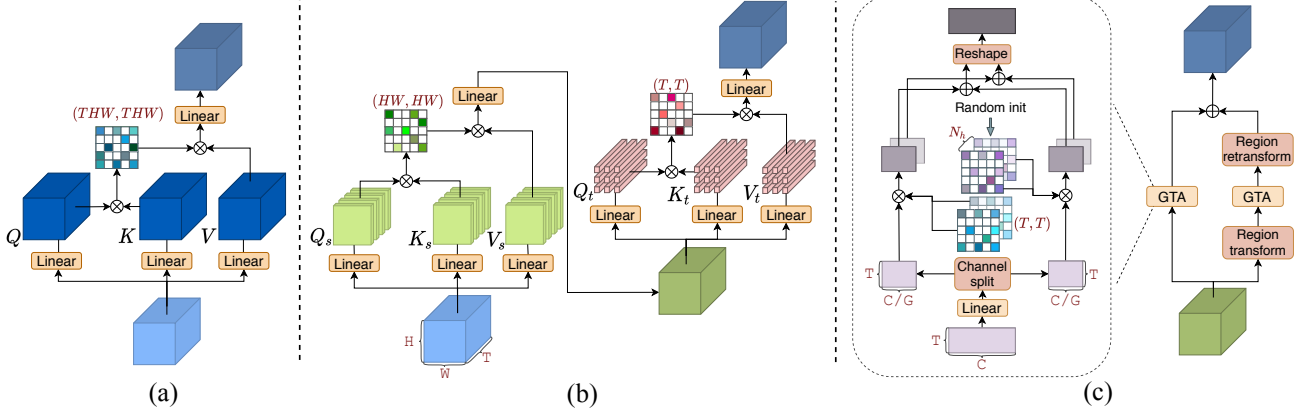


Figure 2: (a) **Standard self-attention for action recognition**, which computes pairwise similarities between a pixel (query) with other pixels (key) in the spacetime domain. (b) **Decoupled spatial and temporal self-attention**, which uses separated key/query/value representations for spatial and temporal attention and aggregates spatial and temporal context in a separate manner. (c) **Global temporal attention**, which learns two randomly initialized global attention maps at the pixel-level and the region-level, respectively. Regions are derived automatically with a learned transformation matrix. Inside the rectangular (dashed line), the spatial dimension of feature maps is omitted. GTA is also applied in a cross-channel multi-head fashion, where feature maps are split along the channel dimension into G groups (only 2 groups are showed for simplicity). See texts for more details.

standing of the attention mechanism utilized in video action recognition.

3. Approach

We start with a brief review of self-attention for video action recognition in Section 3.1. Then, we introduce the decoupling of spatial and temporal modeling in Section 3.2. Finally, we elaborate GTA that is designed for better temporal modeling in Section 3.3.

3.1. Background

Extending the self-attention module [2] for language tasks, the non-local block [6] takes as inputs flattened pixels in spacetime to model pairwise interactions, as shown in Figure 2(a). More formally, given an input feature map $X \in \mathbb{R}^{N \times C}$, three linear projections are applied to obtain key (K), query (Q), and value (V) representations, where C is the channel dimension of the feature map. We use $N = THW$ to denote the total number of positions in both space and time dimensions, where T , H and W are the number of time steps, height and width of the feature map, respectively. The three projections can be written as

$$Q = XW_Q, \quad K = XW_K, \quad V = XW_V, \quad (1)$$

parameterized by three weight matrices $W_Q, W_K, W_V \in \mathbb{R}^{C \times C}$ respectively. The output of the self-attention operation is computed as a weighted sum of the value representations. Here, the weight is defined by the attention weight matrix $M \in \mathbb{R}^{N \times N}$, where each element denotes a scaled

dot product between the query pixel and the corresponding key pixel, followed by a softmax normalization:

$$M = \text{softmax} \left(\frac{QK^T}{\sqrt{C}} \right) \quad (2)$$

$$A = MV \quad (3)$$

The attention output is incorporated into the backbone network via a final linear projection and a residual connection [34]:

$$Y = X + AW_O, \quad (4)$$

where $W_O \in \mathbb{R}^{C \times C}$. An optional normalization layer (e.g., BatchNorm [35] and LayerNorm [36]) can be used before the residual connection, and we drop it here for clarity.

3.2. Decoupled Spatial and Temporal Self-Attention

Although self-attention has been widely used in action recognition for capturing spatio-temporal dependencies, we argue in this paper that the coupled modeling of spatial and temporal self-attention prevents the model from learning effective temporal attention. First, when sharing the same transformation matrices for key, query and value, it fails to differentiate between spatial and temporal contexts. This is unsatisfactory for temporal modeling as we need to consider temporal structures of videos instead of simply computing the salient regions by performing self-attention in the spatial domain. Moreover, when the two attentions are modeled and aggregated jointly, the combined attention tends to be biased towards the appearance similarity as the temporal attention is dominated by the spatial one (see Figure 1

(a). Based on this observation, we propose the decoupled spatial and temporal self-attention in Figure 2 (b), which breaks down the standard self-attention block into a spatial self-attention block followed by a temporal self-attention block. However, it worth noting that self-attention is usually permutation-invariant [8], and thus directly using it fails to consider the ordering information of frames.

3.3. Global Temporal Attention

We now introduce GTA, which is applied on top of a standard spatial self-attention block. GTA aims to learn a global attention map that considers temporal structures and generalizes well for all samples.

Formally, we first reshape the input feature map to be $X \in \mathbb{R}^{T \times HW \times C}$. Pixels in different time steps are considered as different samples, then we perform self-attention for all pixels in the spatial domain (*i.e.*, HW , see Figure 2 (b) left), resulting in a new feature map $\hat{X} \in \mathbb{R}^{T \times HW \times C}$ with the same size of the reshaped X . Then, we reshape \hat{X} to be $\tilde{X} \in \mathbb{R}^{HW \times T \times C}$ by treating pixels in spatial domain as different samples and leverage GTA for temporal modeling along the time axis T .

Unlike standard self-attention where the attention map is produced by pairwise interactions conditioned on input pixels, we train an attention map that does not depend on individual pixels. In particular, we randomly initialize a weight matrix $\hat{M} \in \mathbb{R}^{T \times T}$ to modulate the value representation as:

$$\hat{A} = \hat{M}V. \quad (5)$$

The idea of using a global attention matrix rather than pairwise dot product as in Eqn. 2 is that pairwise interactions fluctuate across different samples, lacking a global temporal consistency at the dataset level. In addition, the standard self-attention fails to consider the ordering of sequences [8]—if we shuffle the pixels used to compute the attention map (*i.e.* Eqn 2), the value between a pair would still be the same in the matrix, thus the output will not change, which is not what we desire.

Cross-channel Multi-head GTA. The attention matrix $M \in \mathbb{R}^{T \times T}$ is used to learn a linear combination of $V \in \mathbb{R}^{T \times C}$ ¹ across different time steps, without considering feature interactions in the channel dimension. We further improve temporal modeling by incorporating channel interactions. We split C into G groups, and for each group and we apply a multi-head GTA. In particular, for the g -th group, the outputs of the multi-head attention MH_g can be derived as:

$$MH_g = \text{Concat}_{k=1}^{N_h} (\hat{M}_g^k V_g) \in \mathbb{R}^{N_h \times T \times \lfloor \frac{C}{G} \rfloor}, \quad (6)$$

¹ HW are considered as different samples and we omit it for brevity.

where $\hat{M}_g^k \in \mathbb{R}^{T \times T}$ represents the k -th head for the g -th group, $V_g \in \mathbb{R}^{T \times \lfloor \frac{C}{G} \rfloor}$ denotes the value for the g -th group and N_h denotes the number of heads used. Each head focuses on distinct temporal attention patterns. To capture interactions across different groups, we sum the outputs along the channel dimension between different groups to produce MH_G as:

$$MH_G = \sum_{g=1}^G MH_g \in \mathbb{R}^{N_h \times T \times \lfloor \frac{C}{G} \rfloor}, \quad (7)$$

which mixes information across channels in different groups. In order for MH_G to have the same size as $\hat{X} \in \mathbb{R}^{T \times C}$ ¹ for residual addition, one can transform MH_G with an additional layer. Instead, we simply set N_h to be G and reshape MH_G to be the same size of $\mathbb{R}^{T \times C}$.

Temporal Modeling for Pixels and Regions. Recall that we apply the GTA module by treating all pixels in the space domain individually (*i.e.*, HW) as different samples. In addition to that, we project spatial domain HW into different regions by learning a region transformation matrix $W_R \in \mathbb{R}^{T \times R \times HW}$ to map $\hat{X} \in \mathbb{R}^{T \times HW \times C}$ to $\tilde{X} \in \mathbb{R}^{T \times R \times C}$. The intuition is to group similar pixels with related semantic meanings into the same region. And we wish to learn temporal relationships not only at the pixel level but also at the region level. Therefore, we apply the cross-channel multi-head GTA in a similar fashion. The output of the region GTA is multiplied with the reversed region transformation matrix to match the size of the input, which we just reuse the transposed transformation matrix W_R^T . Finally, the outputs of the global temporal attention module can be written as:

$$Y = \hat{X} + \underbrace{MH_G(\hat{X})W_O^P}_{\text{GTA on pixels}} + \underbrace{W_R^T MH_G(\tilde{X})W_O^R}_{\text{GTA on regions}}. \quad (8)$$

Here, the second and the third term denote our GTA module on pixels and regions, respectively. W_O^P and W_O^R transforms the output of Pixel GTA and Region GTA to be added with \hat{X} in a residual manner.

4. Experiments

4.1. Experimental Setups

Datasets. We evaluate our approach on three video action benchmarks, including two temporal-related datasets: Something-Something v1 (SSv1) and Something-Something v2 (SSv2) [9], and a dataset that is less sensitive to temporal relationships: Kinetics-400 (K400) [37]. In detail, Something-Something v1&v2 include 110K and 220K videos respectively over 174 action classes. Kinetics-400 is a large-scale human action recognition dataset with 400

classes, which contains 300K YouTube video clips. As stated in [18, 38], actions in Kinetics datasets can be easily determined from the background clues instead of temporal information. As we aim to improve temporal modeling for video action recognition, our experiments focus more on temporal sensitive datasets (SSv1 and SSv2).

Implementation Details. GTA is flexible and can be easily inserted into existing 2D and 3D backbones. In our experiments, we adopt the standard R2D-50 network [34] and the SlowFast-R50 network [7] as our 2D/3D backbones. The 2D CNN backbone networks are initialized with ImageNet [39] pre-trained weights, and the 3D CNN backbone networks are pre-trained on Kinetics-400 [10]. The GTA module is initialized with Kaiming initialization [40].

For experiments using 2D CNN backbones, we train the model following the TSN [12] sampling strategy, which divides the input video into multiple segments and averages the frame-level features extracted from each segment for video-level action classification. We also apply the same data augmentation as TSN, which first resizes the input frames to 240×320 pixels, followed by the multi-scale cropping and random flipping, and then resizes the cropped regions to 224×224 pixels. Unless otherwise stated, we use 8 frames as inputs for experiments on 2D CNN backbones for SSv1 and SSv2 datasets.

For experiments with 3D CNN backbones, we follow the same sampling practice and training/testing strategy in previous work [7]. Specifically, we apply the scale-jitter with a shorter side sampled in [256, 340] pixels and then randomly crop a region of 224×224 pixels size.

During testing, on SSv1 and SSv2 datasets, we sample 1 clip from each video and the center crop of size 224×224 pixels for evaluation. We keep the same protocol for the methods compared in the same table. On the Kinetics-400 dataset, we sample 10 clips in the temporal domain and 3 crops in the spatial domain with full resolution of size 256×256 pixels. More dataset-specific training and testing details are available in the supplementary material.

4.2. Main Results

Effectiveness of GTA in a decoupled framework. We report the results of GTA using both 2D and 3D backbones and compare with the alternative approaches: (1) non-local module (NL) [6], which is a variant of self-attention that flattens all pixels in space and time dimension into a huge vector; (2) decoupled non-local module (DNL), which breaks down the non-local module into a spatial self-attention followed by temporal self-attention. For both of our approaches and the compared baselines, we apply five (2 to res_3 and 3 to res_4 for every other residual block) blocks in the backbone networks unless specified, following [6].

Table 1 summarizes the comparison results. We first observe a huge gap between the performance of 2D and

Table 1: Comparisons with the non-local block. Top-1 accuracy (%) on validation datasets are reported here.

Model	GFLOPs	#Params	SSv1	SSv2
2D backbone	32.7	23.9 M	17.0	26.8
+ NL	61.1	31.2 M	31.2	50.7
+ DNL	49.9	31.2 M	38.8	55.5
+ GTA	50.2	31.2 M	50.6	63.5
3D backbone	131.4	34.0 M	50.9	63.4
+ NL	239.9	41.4 M	51.7	63.9
+ DNL	169.1	41.4 M	52.0	64.1
+ GTA	169.9	41.4 M	53.4	64.9

3D backbones, which shows the importance of utilizing temporal information for SSv1&SSv2 datasets. While NL achieves better performance than vanilla 2D models, the improvements are less significant (less than 1%) on 3D models compared to the 2D backbone. This suggests that NL is ineffective for models that already capture temporal relationships among different frames by 3D convolutions.

Notably, we see that by simply separating temporal self-attention from spatial self-attention, DNL outperforms NL on both backbones, while requiring 20%-30% less computation cost. Specifically, compared to NL, DNL offers a 7.6% / 4.8% gain on SSv1 and SSv2, respectively in the 2D setting. This suggests that the spatial and temporal self-attentions should be treated separately to capture more informative temporal contexts. We further visualize the attention maps obtained by NL and DNL in Figure 3. The first row in each example shows the attention maps obtained by the NL, which includes spatio-temporal attention between the query position and all other positions in the entire video. The second and third rows show the attention maps obtained by DNL, including a spatial attention map within the query frame and a temporal attention map at the query position over the whole sequence. We observe that the attention maps obtained by the NL mostly focus on the same object across input frames (*i.e.*, the pen, the hand). This implies that the spatio-temporal attention in NL mostly concentrates on capturing the appearance similarities instead of the temporal relations within the video sequence. In contrast, by decoupling them, the module is capable of capturing effective temporal dependencies by attending to the frames which are critical for recognizing the actions. For example, in Figure 3(b), the temporal attention weights are large in the last few frames where the action "tearing something" is happening.

Finally, GTA produces the best results on datasets with both 2D and 3D backbones. For example, with the 2D backbone, GTA further outperforms DNL by 11.8% / 8.0%

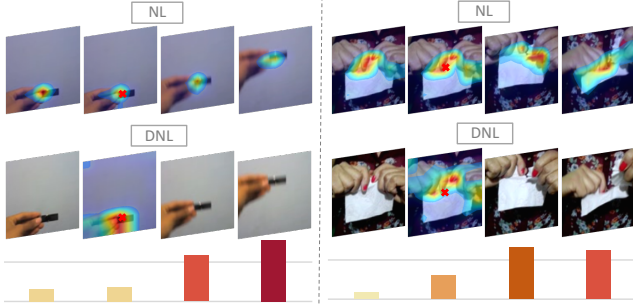


Figure 3: Visualization of the attention maps of two examples: (a)“Moving something up”; (b)“Tearing something into two pieces”. The first row shows the generated spatio-temporal attention map by the non-local module. The second and third row is the spatial and temporal attention map obtained by the decoupled non-local module. The red cross mark denotes the queried position.

on SSV1, SSV2, respectively, confirming the effectiveness of GTA for temporal modeling. With a 3D backbone, we observe similar trends with smaller gains, since GTA is built upon a stronger baseline with temporal information extracted by 3D convolutions. This highlights the compatibility of GTA for both 2D and 3D networks. It is also noteworthy that 2D networks can achieve comparable performance with 3D backbones when equipped with GTA.

4.3. Discussion

Impact of inserting positions and number of modules. Table 2 explores the performance of different inserting positions and the number of modules inserted. We see that even a single module inserted at res_3 or res_4 can bring significant improvement over the baseline. However, the enhancement on res_5 is minor. We hypothesize that the final residual layer loses too much fine-grained spatial information, which may hinder the learning of temporal attention at the pixel-level and the region-level.

Table 2: Impact of inserting positions and number of blocks.

res_3	res_4	res_5	Top-1	Top-5
			17.0	44.6
+1			46.2	74.8
	+1		46.4	75.3
		+1	37.4	66.6
+1	+1		49.5	77.8
+2	+3		50.6	78.8

Impact of Spatial and Temporal Attention. In Table 3, we perform ablation studies to validate the contribution of

each component in the framework. Based on a R2D-50, we compare the use of, (1) SA, a vanilla spatial self-attention; (2) TA, a vanilla temporal self-attention; (3) TAPE, a vanilla temporal self-attention with positional encodings on time dimension [2]; (4) PIXEL GTA, which performs GTA on flattened pixels on the time axis; (5) REGION GTA, which applies GTA to regions. Additionally, we use “+” to denote different combinations of these methods. The results are summarized in Table 3. As the SSV1 dataset relies highly on temporal relationships, applying spatial self-attention (SA) alone in the spatial domain slightly improves the backbone network (0.9% gain), while using the temporal self-attention module (TA) provides much more significant improvements (20.6% gain). We also see that combining spatial attention with temporal attention offers performance gains. In addition, our GTA is able to improve the vanilla TA block by a large margin (10.9% with Pixel GTA and 9.5% with Region GTA), which demonstrates the superior effectiveness of our design to capture temporal information.

Table 3: Impact of spatial and temporal attention blocks.

Model	Top-1	Δ
R2D-50	17.0	-
+ SA	17.9	+0.9
+ TA	37.6	+20.6
+ Pixel GTA	48.5	+31.5
+ Region GTA	47.1	+30.1
+ SA + TA	38.8	+21.8
+ SA + TAPE	48.4	+31.4
+ SA + Pixel GTA	49.2	+32.2
+ SA + Region GTA	47.9	+30.9
+ SA + Pixel & Region GTA	50.6	+33.6

Adding positional encoding to the vanilla TA block can largely improve the performance by 9.6%, which proves the importance of temporal ordering information. However, the performance of TAPE is still lower than Pixel GTA, which demonstrates the superiority of our GTA design. Comparing across different GTA variants, we see that Pixel GTA is slightly better than the Region GTA. Additionally, when these two modules are combined together, we observe at least 1.4% improvement compared to using each of them alone. It indicates that Pixel GTA and Region GTA are complementary to each other, focusing on learning temporal relationships at different spatial levels.

We further visualize regions that are automatically discovered by Region GTA in Figure 4. We can see that Region GTA can discover regions that share similar semantic mean-

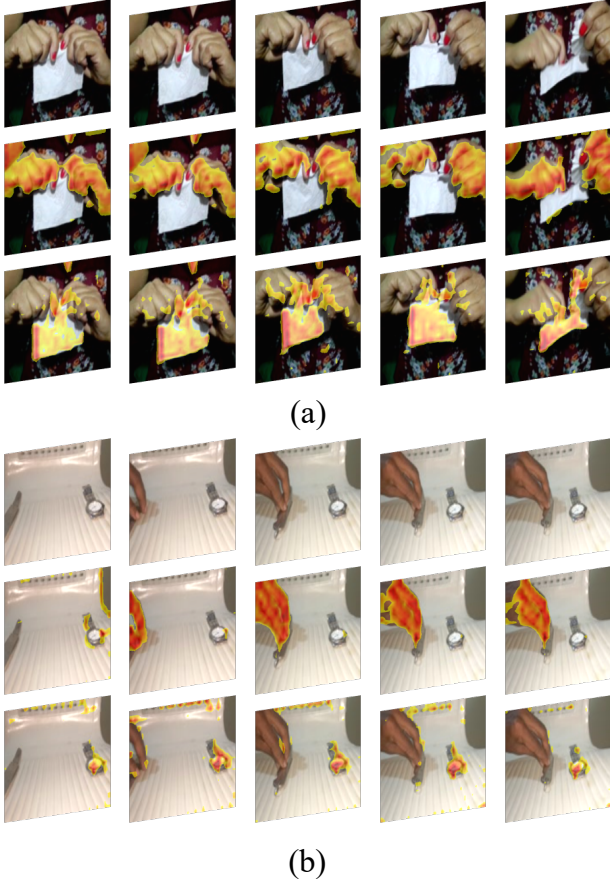


Figure 4: Visualization of transformed regions: (a)“Tearing something into two pieces”; (b)“Moving something closer to something”. The first row is the frame sequences. The second and third rows are regions obtained by Region GTA.

ings. For example, in the first video, the “hand” region and the “paper” region are automatically identified, while the “hand” and the “watch” are detected in the second video.

Table 4: Impact of group count. Top-1 accuraries on validation datasets are reported here.

Group count	SSv1	SSv2
1	47.5	62.6
2	49.8	63.4
4	50.4	63.4
8	50.6	63.5
16	50.0	63.2

Impact of Group Count in Cross-channel Multi-head GTA. We evaluate different values of group count used in GTA on SSv1 and SSv2 datasets. The results are summarized in Table 4. We can see that when the group count

Table 5: Comparisons with state-of-the-art methods on Kinetics-400 dataset.

Method	GFLOPs \times views	Top-1	Top-5
TSN [12]	80 \times 10	72.5	90.2
TSM [20]	86 \times 30	74.7	91.4
bLVNet-TAM [41]	93 \times 9	73.5	91.2
MSNet [42]	87 \times 10	76.4	-
Two-Stream R(2+1)D [43]	304 \times 115	75.4	91.9
Two-Stream S3D-G [38]	143 \times N/A	77.2	93.0
I3D+NL [6]	359 \times 30	77.7	93.3
SlowFast-R101 [7]	106 \times 30	77.9	93.2
CorrNet-R101 [44]	224 \times 30	79.2	-
C2D-R50 + NL	77 \times 30	74.8	91.5
C2D-R50 + GTA	62 \times 30	75.9	92.2
SlowFast-R101 + NL	137 \times 30	78.9	93.9
SlowFast-R101 + GTA	137 \times 30	79.8	94.1

is larger than 1, which enables channel interactions among different groups. It can largely improve the performance on both SSv1 and SSv2 datasets, which demonstrates the importance of channel interactions in GTA. And a group count of 8 offers the best performance on SSv1 and SSv2. When the group count becomes larger than 8, the performance drops. We conjecture that too many channel interactions increase the optimization difficulty.

4.4. Comparisons with State-of-the-art.

Kinetics-400 Table 5 presents the comparative results with other state-of-the-art methods on Kinetics-400. The first section of the table shows the methods based on 2D CNN network. The second section contains the models with 3D CNN backbone. The third section illustrates the comparison of our GTA and NL added to 2D and 3D CNN backbones. We can see that GTA can achieve consistent improvement over the NL counterpart on 2D and 3D CNN backbones. And adding GTA to SlowFast-R101 can achieve 79.8% top-1 accuracy on Kinetics-400 dataset, which is the state-of-the-art performance on Kinetics-400.

Something-Something v1&v2 We also compare our approach with the state-of-the-art methods on SSv1 & SSv2 datasets. As is shown in Table 7, given 8 input frames, our approach based on 2D RestNet-50 with TSM backbone achieves 51.6% and 63.7% on SSv1 and SSv2 at top-1 accuracy, respectively. Specifically, on SSv1 and SSv2 datasets, with the same number of input frames, our approach outperforms the TRN [18] which utilizes relation

Table 6: Comparisons with state-of-the-art methods on Something-Something v1 & v2 datasets. **Bold** and underline shows the highest and second highest results.

Method	Backbone	Pretrain	Frames×Crops ×Clips	SSv1		SSv2	
				Val Top-1	Val Top-5	Val Top-1	Val Top-5
TSN [12]	2D R50	ImgNet	8×1×1	19.7	46.6	30.0	60.5
TRN [18]	BNInception	ImgNet	8×1×1	34.4	-	48.8	-
TSM [20]	2D R50	ImgNet	8×1×1	45.6	74.2	58.8	85.4
TSM [20]	2D R50	ImgNet	16×1×1	47.3	77.1	61.2	86.9
TSM _{RGB+Flow} [20]	2D R50	ImgNet	(16+16)×1×1	52.6	81.9	65.0	89.4
MSNet [42]	2D R50+TSM	ImgNet	8×1×1	50.9	80.3	63.0	88.4
MSNet [42]	2D R50+TSM	ImgNet	16×1×1	52.1	82.3	64.7	89.4
MSNet _{En} [42]	2D R50+TSM	ImgNet	(16+8)×1×10	<u>55.1</u>	84.0	<u>67.1</u>	<u>91.0</u>
ECO [45]	3D R18+BNInc	K400	16×1×1	41.4	-	-	-
ECO _{En} Lite [45]	BNInc+3D R18	K400	92×1×1	46.4	-	-	-
I3D [37]	3D R50	K400	32×3×2	41.6	72.2	-	-
I3D+NL [6]	3D R50	K400	32×3×2	44.4	76.0	-	-
I3D+NL+GCN [46]	3D R50	K400	32×3×2	46.1	76.8	-	-
S3D-G [38]	3D Inception	ImgNet	64×1×1	48.2	78.7	-	-
CorrNet [44]	3D CorrNet-50	-	32×1×10	48.5	-	-	-
CorrNet [44]	3D CorrNet-101	-	32×3×10	51.1	-	-	-
TEA [47]	3D R50	ImgNet	8×1×1	48.9	78.1	-	-
TEA [47]	3D R50	ImgNet	16×3×10	52.3	81.9	65.1	89.9
GTA	2D R50	ImgNet	8×1×1	50.6	78.8	63.5	88.6
GTA	2D R50	ImgNet	16×1×1	52.0	80.5	64.7	89.3
GTA	2D R50+TSM	ImgNet	8×1×1	51.6	79.8	63.7	88.9
GTA	2D R50+TSM	ImgNet	16×1×1	53.7	81.7	65.3	89.6
GTA_{En}	2D R50+TSM	ImgNet	(16+8)×3×2	56.5	<u>83.1</u>	68.1	91.1

networks, and MSNet [42] which incorporates the motion features. This demonstrates that our proposed GTA is more effective in modeling temporal relationships. Our approach also achieves superior results when compared with the recent work that leverages additional modules to improve 3D CNN backbones, such as the non-local block (I3D+NL [6]), GCN (I3D+NL+GCN [46]), the correlation operation (CorrNet [44]), and the multiple temporal aggregation module and the motion excitation module (TEA [47]). Finally, we evaluate the ensemble model (GTA_{En}) by averaging output prediction scores of the 8-frame and 16-frame models, and obtain 56.5% and 68.1% at top-1 accuracy on SSv1 and SSv2, respectively, which achieves the state-of-the-art performance on both of the datasets.

5. Conclusion

In this paper, we first demonstrated that by simply disentangling temporal self-attention from spatial self-attention,

significant performance gains can be achieved over standard self-attention methods for video action recognition tasks. We then presented Global Temporal Attention (GTA) for superior temporal modeling, which is applied on top of spatial self-attention. Unlike standard self-attention that generates attention maps based on pairwise interactions conditioned on each sample, GTA randomly initializes a global attention map and learns global temporal structures that generalize well across different samples. To further improve temporal modeling, GTA is designed in a cross-channel multi-head fashion that models the channel interactions among several groups. Additionally, GTA is not only applied to pixels at the same spatial location but also on regions of similar semantic meanings, which are automatically discovered with a learned transformation matrix. Experimental results demonstrate that our approach is more effective for temporal modeling and achieves state-of-the-art results on three challenging video action benchmarks.

Acknowledgements. This work was supported by the Air Force (STTR awards FA865019P6014, FA864920C0010), and an independent gift from Facebook AI.

References

- [1] Dzmitry Bahdanau, Kyunghyun Cho, and Yoshua Bengio. Neural machine translation by jointly learning to align and translate. *arXiv preprint arXiv:1409.0473*, 2014. 1
- [2] Ashish Vaswani, Noam Shazeer, Niki Parmar, Jakob Uszkoreit, Llion Jones, Aidan N Gomez, Łukasz Kaiser, and Illia Polosukhin. Attention is all you need. In *NeurIPS*, 2017. 1, 2, 3, 6
- [3] Jan K Chorowski, Dzmitry Bahdanau, Dmitriy Serdyuk, Kyunghyun Cho, and Yoshua Bengio. Attention-based models for speech recognition. In *NeurIPS*, 2015. 1
- [4] Jie Hu, Li Shen, and Gang Sun. Squeeze-and-excitation networks. In *CVPR*, 2018. 1, 2
- [5] Jie Hu, L Longfei Shen, Samuel Albanie, Gang Sun, and Andrea Vedaldi. Gather-excite: Exploiting feature context in convnets. In *NeurIPS*, 2018. 1, 2
- [6] Xiaolong Wang, Ross B. Girshick, Abhinav Gupta, and Kaiming He. Non-local neural networks. In *CVPR*, 2017. 1, 2, 3, 5, 7, 8
- [7] Christoph Feichtenhofer, Haoqi Fan, Jitendra Malik, and Kaiming He. Slowfast networks for video recognition. In *ICCV*, 2019. 1, 2, 5, 7, 11
- [8] Jean-Baptiste Cordonnier, Andreas Loukas, and Martin Jaggi. On the relationship between self-attention and convolutional layers. In *ICLR*, 2020. 2, 4
- [9] Raghav Goyal, Samira Ebrahimi Kahou, Vincent Michalski, Joanna Materzynska, Susanne Westphal, Heuna Kim, Valentin Haenel, Ingo Fruend, Peter Yianilos, Moritz Mueller-Freitag, et al. The” something something” video database for learning and evaluating visual common sense. In *ICCV*, 2017. 2, 4, 11
- [10] Will Kay, Joao Carreira, Karen Simonyan, Brian Zhang, Chloe Hillier, Sudheendra Vijayanarasimhan, Fabio Viola, Tim Green, Trevor Back, Paul Natsev, et al. The kinetics human action video dataset. *arXiv preprint arXiv:1705.06950*, 2017. 2, 5
- [11] Andrej Karpathy, George Toderici, Sanketh Shetty, Thomas Leung, Rahul Sukthankar, and Li Fei-Fei. Large-scale video classification with convolutional neural networks. In *CVPR*, 2014. 2
- [12] Limin Wang, Yuanjun Xiong, Zhe Wang, Yu Qiao, Dahua Lin, Xiaoou Tang, and Luc Van Gool. Temporal segment networks: Towards good practices for deep action recognition. In *ECCV*, 2016. 2, 5, 7, 8, 11
- [13] Rohit Girdhar, Deva Ramanan, Abhinav Gupta, Josef Sivic, and Bryan Russell. Actionvlad: Learning spatio-temporal aggregation for action classification. In *CVPR*, 2017. 2
- [14] Shuiwang Ji, Wei Xu, Ming Yang, and Kai Yu. 3d convolutional neural networks for human action recognition. *PAMI*, 2012. 2
- [15] Du Tran, Lubomir Bourdev, Rob Fergus, Lorenzo Torresani, and Manohar Paluri. Learning spatiotemporal features with 3d convolutional networks. In *ICCV*, 2015. 2
- [16] Jeff Donahue, Lisa Anne Hendricks, Sergio Guadarrama, Marcus Rohrbach, Subhashini Venugopalan, Trevor Darrell, and Kate Saenko. Long-term recurrent convolutional networks for visual recognition and description. In *CVPR*, 2015. 2
- [17] Joe Yue-Hei Ng, Matthew Hausknecht, Sudheendra Vijayanarasimhan, Oriol Vinyals, Rajat Monga, and George Toderici. Beyond short snippets: Deep networks for video classification. In *CVPR*, 2015. 2
- [18] Bolei Zhou, Alex Andonian, Aude Oliva, and Antonio Torralba. Temporal relational reasoning in videos. In *ECCV*, 2018. 2, 5, 7, 8, 11
- [19] Noureldien Hussein, Efstratios Gavves, and Arnold WM Smeulders. Timeception for complex action recognition. In *CVPR*, 2019. 2
- [20] Ji Lin, Chuang Gan, and Song Han. Tsm: Temporal shift module for efficient video understanding. In *ICCV*, 2019. 2, 7, 8, 11
- [21] Thomas M Strat and Martin A Fischler. Context-based vision: recognizing objects using information from both 2 d and 3 d imagery. *PAMI*, 1991. 2
- [22] Antoni Buades, Bartomeu Coll, and J-M Morel. A non-local algorithm for image denoising. In *CVPR*, 2005. 2
- [23] Alexei A Efros and Thomas K Leung. Texture synthesis by non-parametric sampling. In *ICCV*, 1999. 2
- [24] Saurabh Gupta, Bharath Hariharan, and Jitendra Malik. Exploring person context and local scene context for object detection. *arXiv preprint arXiv:1511.08177*, 2015. 2
- [25] Jeremy Heitz and Daphne Koller. Learning spatial context: Using stuff to find things. In *ECCV*, 2008. 2
- [26] Roozbeh Mottaghi, Xianjie Chen, Xiaobai Liu, Nam-Gyu Cho, Seong-Whan Lee, Sanja Fidler, Raquel Urtasun, and Alan Yuille. The role of context for object detection and semantic segmentation in the wild. In *CVPR*, 2014. 2
- [27] Han Zhang, Ian Goodfellow, Dimitris Metaxas, and Augustus Odena. Self-attention generative adversarial networks. *arXiv preprint arXiv:1805.08318*, 2018. 2
- [28] Yue Cao, Jiarui Xu, Stephen Lin, Fangyun Wei, and Han Hu. Gcnet: Non-local networks meet squeeze-excitation networks and beyond. In *ICCVW*, 2019. 2
- [29] Han Hu, Jiayuan Gu, Zheng Zhang, Jifeng Dai, and Yichen Wei. Relation networks for object detection. In *CVPR*, 2018. 2
- [30] Hang Zhang, Kristin Dana, Jianping Shi, Zhongyue Zhang, Xiaogang Wang, Amrith Tyagi, and Amit Agrawal. Context encoding for semantic segmentation. In *CVPR*, 2018. 2
- [31] Adam Santoro, David Raposo, David G. T. Barrett, Mateusz Malinowski, Razvan Pascanu, Peter W. Battaglia, and Timothy P. Lillicrap. A simple neural network module for relational reasoning. In *NeurIPS*, 2017. 2

- [32] Jun Fu, Jing Liu, Haijie Tian, Yong Li, Yongjun Bao, Zhiwei Fang, and Hanqing Lu. Dual attention network for scene segmentation. In *CVPR*, 2019. [2](#)
- [33] Zilong Huang, Xinggang Wang, Lichao Huang, Chang Huang, Yunchao Wei, and Wenyu Liu. Ccnet: Criss-cross attention for semantic segmentation. In *ICCV*, 2019. [2](#)
- [34] Kaiming He, Xiangyu Zhang, Shaoqing Ren, and Jian Sun. Deep residual learning for image recognition. In *CVPR*, 2016. [3](#), [5](#)
- [35] Sergey Ioffe and Christian Szegedy. Batch normalization: Accelerating deep network training by reducing internal covariate shift. *arXiv preprint arXiv:1502.03167*, 2015. [3](#)
- [36] Jimmy Lei Ba, Jamie Ryan Kiros, and Geoffrey E Hinton. Layer normalization. *arXiv preprint arXiv:1607.06450*, 2016. [3](#)
- [37] Joao Carreira and Andrew Zisserman. Quo vadis, action recognition? a new model and the kinetics dataset. In *CVPR*, 2017. [4](#), [8](#), [11](#)
- [38] Saining Xie, Chen Sun, Jonathan Huang, Zhuowen Tu, and Kevin Murphy. Rethinking spatiotemporal feature learning: Speed-accuracy trade-offs in video classification. In *ECCV*, 2018. [5](#), [7](#), [8](#)
- [39] Jia Deng, Wei Dong, Richard Socher, Li-Jia Li, Kai Li, and Li Fei-Fei. Imagenet: A large-scale hierarchical image database. In *CVPR*, 2009. [5](#)
- [40] Kaiming He, Xiangyu Zhang, Shaoqing Ren, and Jian Sun. Delving deep into rectifiers: Surpassing human-level performance on imagenet classification. In *ICCV*, 2015. [5](#)
- [41] Quanfu Fan, Chun-Fu Richard Chen, Hilde Kuehne, Marco Pistoia, and David Cox. More is less: Learning efficient video representations by big-little network and depthwise temporal aggregation. In *NeurIPS*, 2019. [7](#), [11](#)
- [42] Heeseung Kwon, Manjin Kim, Suha Kwak, and Minsu Cho. Motionsqueeze: Neural motion feature learning for video understanding. In *ECCV*, 2020. [7](#), [8](#)
- [43] Du Tran, Heng Wang, Lorenzo Torresani, Jamie Ray, Yann LeCun, and Manohar Paluri. A closer look at spatiotemporal convolutions for action recognition. In *CVPR*, 2018. [7](#)
- [44] Heng Wang, Du Tran, Lorenzo Torresani, and Matt Feiszli. Video modeling with correlation networks. In *CVPR*, 2020. [7](#), [8](#)
- [45] Mohammadreza Zolfaghari, Kamaljeet Singh, and Thomas Brox. Eco: Efficient convolutional network for online video understanding. In *ECCV*, 2018. [8](#), [11](#)
- [46] Xiaolong Wang and Abhinav Gupta. Videos as space-time region graphs. In *ECCV*, 2018. [8](#), [11](#)
- [47] Yan Li, Bin Ji, Xintian Shi, Jianguo Zhang, Bin Kang, and Limin Wang. Tea: Temporal excitation and aggregation for action recognition. In *CVPR*, 2020. [8](#), [11](#)
- [48] Boyuan Jiang, MengMeng Wang, Weihao Gan, Wei Wu, and Junjie Yan. Stm: Spatiotemporal and motion encoding for action recognition. In *ICCV*, 2019. [11](#)
- [49] Priya Goyal, Piotr Dollár, Ross Girshick, Pieter Noordhuis, Lukasz Wesolowski, Aapo Kyrola, Andrew Tulloch, Yangqing Jia, and Kaiming He. Accurate, large mini-batch sgd: Training imagenet in 1 hour. *arXiv preprint arXiv:1706.02677*, 2017. [11](#)
- [50] Ilya Loshchilov and Frank Hutter. Sgdr: Stochastic gradient descent with warm restarts. *arXiv preprint arXiv:1608.03983*, 2016. [11](#)

Supplementary Material

In the supplementary material, Section A reports the performance comparison on the test set of Something-Something v1&v2. Section B provides more dataset-specific implementation details on training and testing. Finally, Section C presents visualization results of swapping the attention functions of the spatial and temporal attention blocks and Section D shows more visualization of the transformed regions in Region GTA.

A. Testing Results on Something v1&v2

We compare the performance of our approach on the test set with the state-of-the-art methods on Something-Something v1 & v2 datasets. As is shown in Table 7, our approach based on 2D ResNet-50 with TSM backbone achieves 49.8% and 66.9% on SSv1 and SSv2 at top-1 accuracy, respectively. Although on SSv1 dataset, it is still below the TSM_{RGB+Flow}, TSM_{RGB+Flow} is based on the two-stream network and utilizes additional optical flow information. With only RGB input, our GTA achieves the best performance among the recently proposed STM [48] and bLVNet-TAM [41] on 2D CNN backbone; I3D+NL+GCN [46] and TEA [47] on 3D CNN backbone.

B. Experiment Details

Something-Something v1&v2 [9] For the experiments based on the 2D CNN backbone, we follow the same sampling strategy as TSN [12] to sample 8 frames from the whole video. The same data augmentation is applied as TSN, which first resizes the input frames to 240×320, followed by the multi-scale cropping and random horizontal flipping. Note that we do not flip the clips which include the words “left” or “right” in their class labels (e.g., “pushing something from right to left”). We train the model for 50 epochs and start with a base learning rate of 0.01 with a batch size of 32. The first 2 epochs are used for linear warm-up [49] and the learning rate is reduced by a factor of 10 at 30, 40, 45 epochs. The backbone network is initialized with ImageNet pre-trained weights. For testing, we resize the input images to 240×320 pixels and center crop 224×224 pixels region. We sample 1 clip from each video for the experiments using 2D backbones.

For the experiments based on the 3D CNN backbone, we employ the same training and testing strategy as SlowFast-16×8-R50 [7]. We sample 16 and 64 frames for the slow and fast pathways, respectively.

Kinetics-400 [37] For the experiments based on the 2D CNN backbone, we use C2D-R50 provided in the PySlowFast codebase [7] and follow the same schedule for model training. For the experiments using 3D CNN backbones, we adopt SlowFast-8×8-R101 [7], which samples 8 and

Table 7: Results on test set with state-of-the-art methods of Something-Something v1 & v2 datasets. **Bold** and underline shows the highest and second highest results.

Method	Backbone	Frames	SSv1	SSv2
TRN _{RGB+Flow} [18]	BNInc	8+8	40.7	56.2
TSM [20]	2D R50	16	46.0	64.3
TSM _{RGB+Flow} [20]	2D R50	16+16	50.7	<u>66.6</u>
STM [48]	2D R50	16	43.1	63.5
bLVNet-TAM [41]	2D R101	64	48.9	-
ECO _{En} Lite [45]	BNInc+3D R18	92	42.3	-
I3D+NL+GCN [46]	3D R50	32	45.0	-
TEA [47]	3D R50	16	46.6	63.2
GTA_{En}	2D R50+TSM	16+8	<u>49.8</u>	66.9

32 frames for the slow and fast pathway, respectively. The model is trained from scratch for 196 epochs with a cosine learning rate scheduling [50]. The base learning rate is set to 0.01 for a batch size of 64. We sample 10 clips temporally and 3 crops spatially from each video for testing.

C. Visualization of Swapped Attention

To further verify that different context information is needed for spatial and temporal attention, we present the visualization of the swapped attention maps in Figure 5. Specifically, we swap the attention functions (i.e., query/key/value projections) of the spatial and temporal attention blocks and visualize the attention maps. We can see that after swapping the spatial and temporal attention functions, the generated temporal attention maps focus more on the frames with similar objects instead of the frames that are useful for recognizing the action. For example, in Figure 5(a), the temporal attention weights are larger in the first two frames which share a similar appearance with the same query position (i.e., the pen). Moreover, the spatial attention maps generated by the temporal attention functions also show substantially different patterns than the original ones. The visualization results further verify that different types of context information needed in spatial and temporal attention are captured in the decoupled non-local module.

D. Visualization of Transformed Regions

We present more visualization of the transformed regions in Figure 6. We can see that Region GTA can discover regions that share similar semantic meanings. For example, in the first video, the “ground” region and the “badminton” region are automatically identified, the “paper” and the “edge” are detected in the second video, and the “green gum” and the “hand” are obtained in the third video.

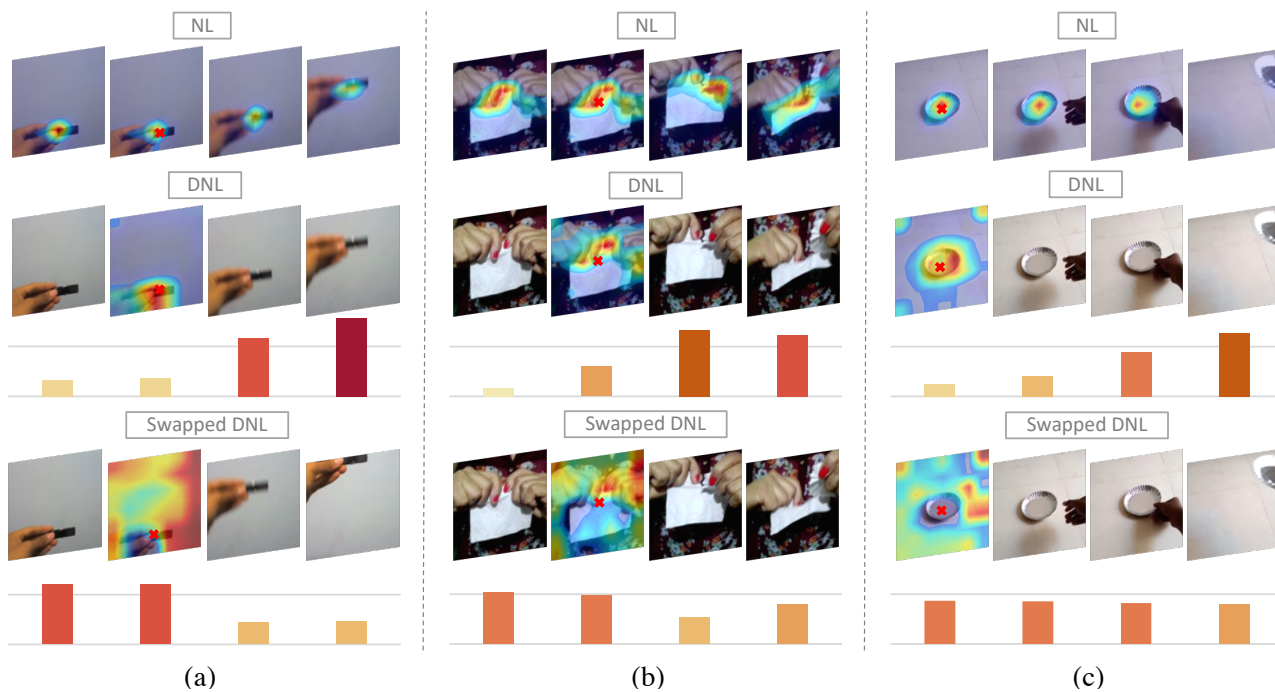


Figure 5: Visualization of the attention maps of three examples: (a)“Moving something up”; (b)“Tearing something into two pieces”; (c)“Picking something up”. The first row is the spatio-temporal attention map generated by the non-local module. The second and third row is the spatial and temporal attention map obtained by our decoupled non-local module. The fourth and fifth row is the spatial and temporal attention map generated by swapping the attention functions of the spatial and temporal attention block. The red cross mark denotes the query position.

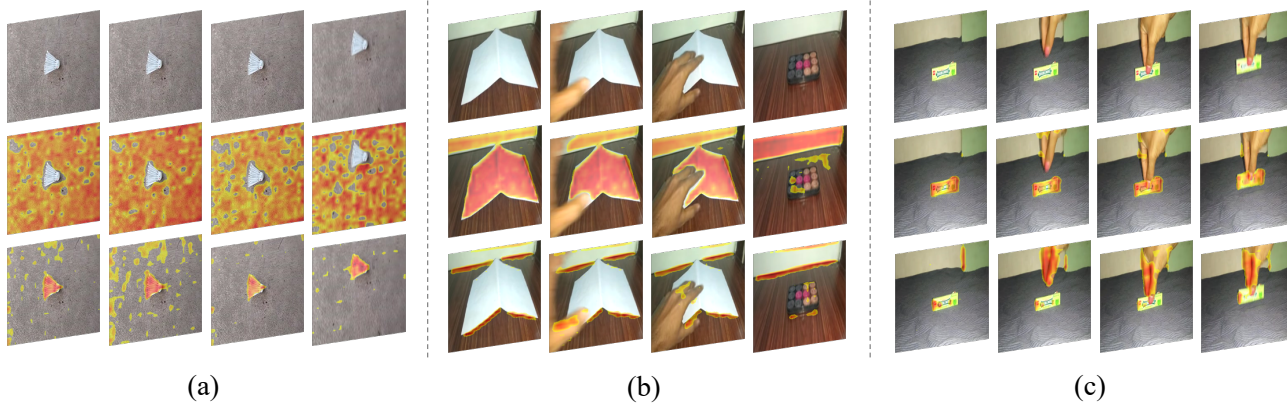


Figure 6: Visualization of the transformed regions of two examples: (a)“Turning the camera downwards while filming something”; (b)“Uncovering something”; (c) “Picking something up”. The first row is the frame sequences. The second and third rows are regions obtained by Region GTA.